

Boundary element method (BEM) model

The two-dimensional nonlinear potential model by Grilli *et al.* (1989,1990), and its most recent extensions, are used to compute wave propagation over the submerged obstacle. With the velocity potential being defined as $\phi(x, t)$, the velocity is given by $u = \nabla\phi = (u, w)$, and the continuity equation in the fluid domain $\Omega(t)$ with boundary $\Gamma(t)$, is a Laplace's equation for the potential,

$$\nabla^2\phi = 0 \quad \text{in } \Omega(t) \quad (1)$$

Using the free space Green's function $G(x, x_l) = -\frac{1}{2\pi} \log |x - x_l|$, equation (1) is transformed into a Boundary Integral Equation (BIE),

$$\alpha(x_l)\phi(x_l) = \int_{\Gamma(x)} \left[\frac{\partial\phi}{\partial n}(x)G'(x, x_l) - \phi(x)\frac{\partial G(x, x_l)}{\partial n} \right] d\Gamma(x) \quad (2)$$

where $x = (x, z)$ and $x_l = (x_l, z_l)$ are position vectors for points on the boundary, n is the unit outward normal vector, and $\alpha(x_l)$ is a geometric coefficient.

On the free surface $\Gamma_f(t)$, ϕ satisfies the full nonlinear kinematic and dynamic boundary conditions,

$$\frac{Dr}{Dt} = \left(\frac{\partial}{\partial t} + u \cdot \nabla \right) r = u = \nabla\phi \quad \text{on } \Gamma_f(t) \quad (3)$$

$$\frac{D\phi}{Dt} = -g\eta + \frac{1}{2}\nabla\phi \cdot \nabla\phi - \frac{p_a}{\rho} \quad \text{on } \Gamma_f(t) \quad (4)$$

respectively, with r , the position vector of a free surface fluid particle, g the acceleration due to gravity, η the vertical elevation of the free surface (positive upwards and $\eta = 0$ at the undisturbed free surface), p_a the pressure at the surface, and ρ the fluid density.

No-flow conditions are prescribed along solid boundaries, and, in the present applications, cnoidal waves are generated on the boundary $\Gamma_{r1}(t)$ by specifying a piston wavemaker motion, as in laboratory experiments (see Grilli & Svendsen 1990, for detail).

The time integration : The time stepping, follows the Eulerian-Lagrangian approach used by Dold & Peregrine 1984. It consists of integrating free surface conditions (3) and (4) at time t , to establish both the new position of the free surface $\Gamma_f(t)$, and the boundary conditions at time $t + \Delta t$ (Δt denotes a small time step increment). Second-order Taylor expansions are expressed in terms of Δt and of the Lagrangian time derivative (as defined in (3)), for both the position $r(t)$ and the potential $\phi(t)$ on the free surface. Coefficients in the series

are calculated by solving two Laplace problems—for ϕ and $\frac{\partial\phi}{\partial t}$ —at each time step (see detail in Grilli, *et al.* 1989).

Numerical implementation : The BIE (2), equivalent to Laplace problems (1) for ϕ , and the equivalent BIE problem for $\frac{\partial\phi}{\partial t}$ are solved by a higher-order BEM, using a set of collocation nodes on the boundary, and elements to interpolate between collocation nodes. Quasi-spline elements are used on the free surface, and isoparametric quadratic elements elsewhere. Each integral in (2) is transformed into a sum of integrals over each boundary element. Non-singular integrals are calculated by standard Gauss quadrature rules. A kernel transformation is applied to the weakly singular integrals, which are then integrated by a numerical quadrature exact for the logarithmic singularity. Details of the numerical implementation can be found in Grilli, *et al.* 1990, along with a discussion of corner problems associated with surface piercing bodies such as wavemakers.

Discretization and numerical parameters : A limitation of the BEM model is that any wave breaking in the computational domain effectively halts the solution algorithm. An adjustment of tank boundaries, hence, had to be made to prevent breaking on the slope of the numerical wave flume. Tank boundaries were re-defined such that the most downwave portion of the slope made the transition to a shallow shelf just below the breaking depth. Fig. 5 shows the re-defined tank boundaries which includes a region of constant depth $h_o = 1$ and length $21h_o$, and a 1:35 slope with a shelf of constant depth $h_1 = 0.34$, at the upper part of the slope, from $x' = \frac{x}{h_o} = 44$ to 56. A rectangular bar of height $0.76h_o$ and width $1.58h_o$ is located with its axis at $x' = 14.83$. As a transmitting boundary condition was not available in the model, reflection off the back wall of the numerical wave flume became a limiting condition. The comparison of BEM model vs. experiments must thus be made in the time between the initiation of paddle motion and the arrival of back wall-reflected energy at the most downwave gage location in the BEM model ($x' = 21$).

The free surface discretization is made of 224 quasi-spline elements, and there are 73 quadratic elements on the bottom and lateral boundaries. The interval between nodes on the free surface is 0.25, and 0.50 on the horizontal bottom, the slope, and the shelf bottom. To increase resolution and accuracy on and above the bar, this interval is reduced to about 0.20 along the bar three sides. The total number of nodes is 365. This corresponds to a CPU time of 7.63sec (IBM3090/300) per time step. Time step is automatically selected in the model, to ensure optimum accuracy and stability of calculations.

BEM model vs. experiment

A comparison is made between computations and experiments, for which both experimental and numerical set-ups correspond to closely identical conditions, with the waves being generated from still water using a piston wavemaker in

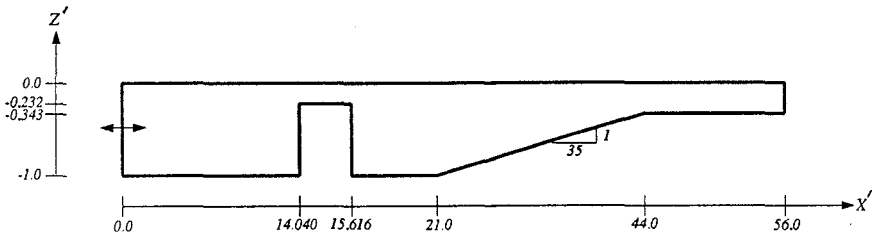


Figure 5: Geometry of the numerical wave flume, as re-defined for entry into BEM model. The shown axes are nondimensionalized with the water depth, $x' = x/h$ and $z' = z/h$.

both cases. In the present case, a cnoidal wave of height $H'_i = \frac{H_i}{h_o} = 0.05$, and period $T' = T \sqrt{\frac{g}{h_o}} = 7.52$ is generated at the leftward lateral boundary of the computational domain, and the corresponding incident wave profile is within 2% of a simple sine wave of length $\frac{L}{h_o} = 6.75$, as measured in the experiments. The model is run for over 20 wave periods, and no adjustment of time lag between both data sets is made before comparison. This, hence, represents a very demanding test of the model performance.

Fig. 6 shows a water surface comparison between the experimental and BEM results. A similar comparison is shown in fig. 7 for time series at locations 0.72 m and 1.92 m downwave of the obstacle. The BEM results are seen to deviate from the experimental results in both amplitude and phase. The nature of this deviation is better revealed by a frequency-domain comparison (fig. 8) which, due to the limitation of the non-breaking BEM requirement, is possible only for the first 8 waveforms following a 10-second startup period. The BEM model is shown to predict harmonics of similar amplitude to those observed in the experiments, with the exception of the first harmonic, which is overpredicted.

This discrepancy in first harmonic amplitude is likely due to the influence of flow separation as the wave-induced velocity oscillations interacted with the corners of the submerged obstacle. As such flow separation was observed in the experiments, the disagreement in the first harmonic amplitude between the BEM model and experiment is not surprising, given the inviscid potential flow assumptions of the model.

As a check, the flow separation loss incurred as a waveform passes the obstacle may be estimated with a crude analytical approach. A simple nonlinear friction representation is assumed, $\eta_1 - \eta_2 = \frac{f}{2g} |u|u$. If the obstacle is assumed thin in relation to the wavelength, quasi-steady flow is assumed, and frictional

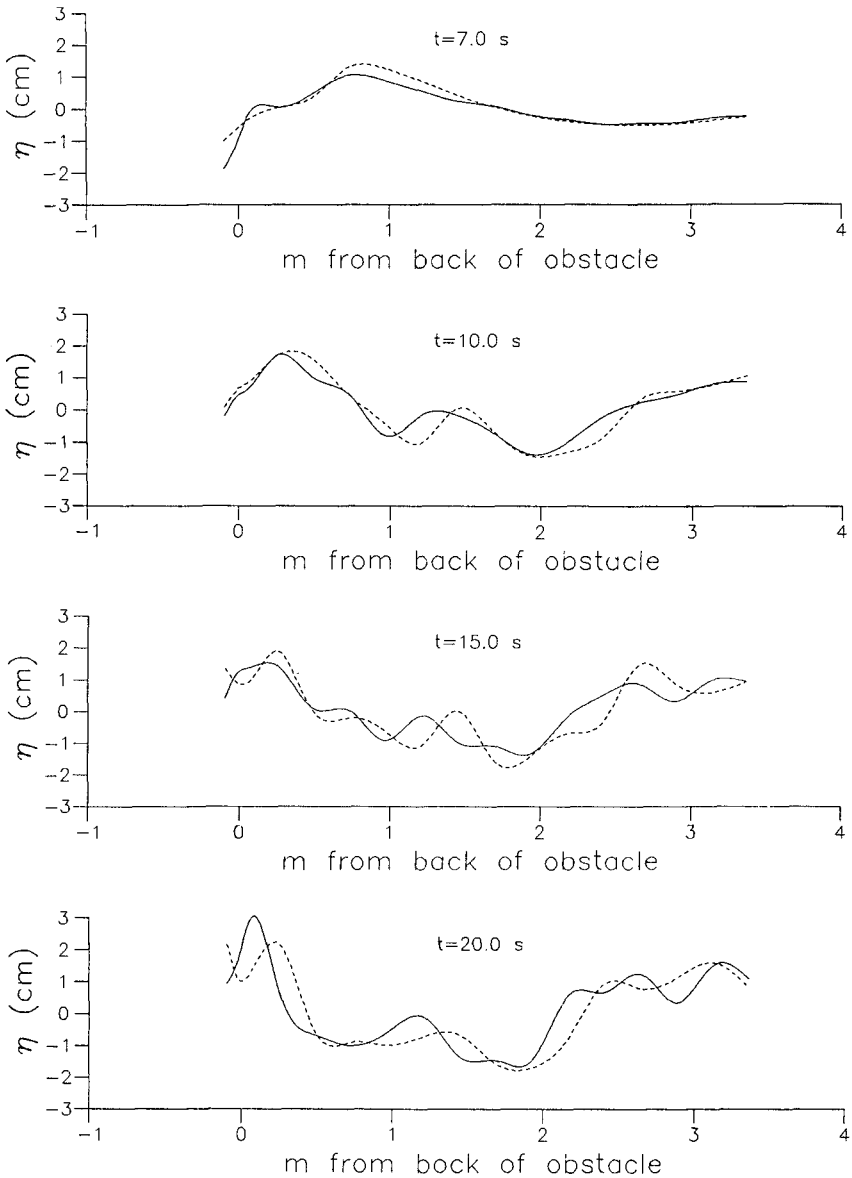


Figure 6: Water surface comparison of BEM model to experiment at $t=7.0$ s, $t=10.0$ s, $t=15.0$ and $t=20.0$ s after the initiation of paddle motion; (---)=BEM model, (—)=experiment.

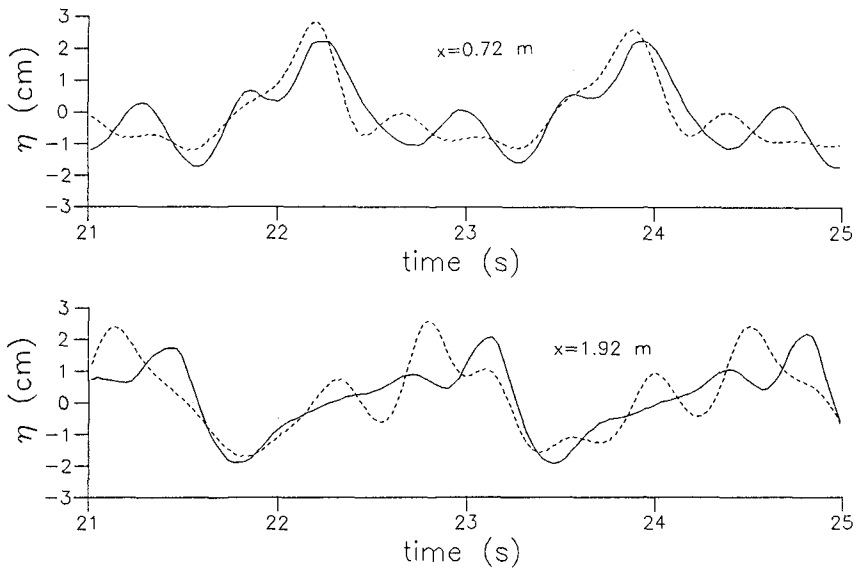


Figure 7: Time series comparison of BEM model data to experiment, at locations 0.72 m and 1.92 m downwave of obstacle; (---)=BEM model, (—)=experiment.

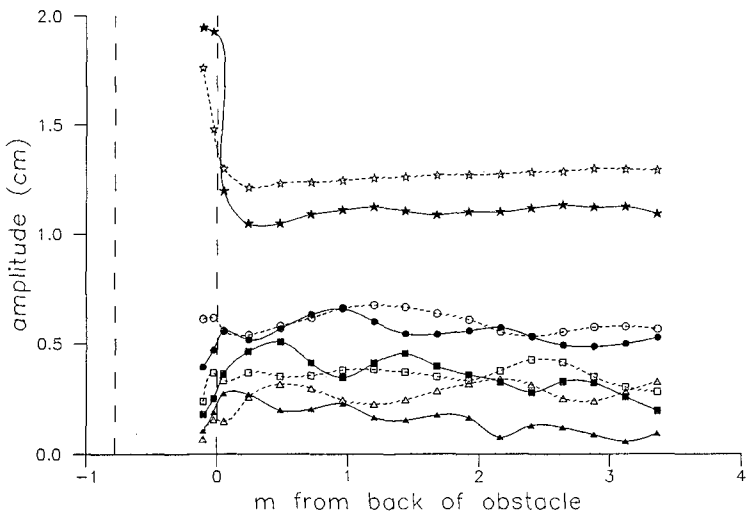


Figure 8: Comparison of spatial amplitude modulations, BEM model and experiment; (---)=BEM model, (—)=experiment, (\star, \star)=1st harmonic, (\bullet, \circ)=2nd harmonic, (\blacksquare, \square)=3rd harmonic, ($\blacktriangle, \triangle$)=4th harmonic.

effects are averaged over a wavelength, it may be shown that

$$\eta_1 - \eta_2 = \frac{4(h/h_o - 1)^2 a^2}{3\pi h_o^2 \omega^2 \cosh^2 kh} [\sinh kh - \sinh k(h - h_o)]^2 \quad (5)$$

where η_1 and η_2 are the water surface elevations prior to and after the obstacle, f is an empirical friction-loss coefficient, u is the amplitude of the depth-averaged velocity downwave of the obstacle, a and h are the amplitude and depth behind the obstacle and h_o is the depth on top of the obstacle. The friction coefficient f for this case is given by $f = (h/h_o - 1)^2$.

Introducing the downwave first harmonic amplitude from the BEM results (~ 1.25 cm) and the other relevant parameters into 5, we find $\eta_1 - \eta_2 \simeq 0.16$ cm. This agrees well with the discrepancy between BEM and experimental amplitudes of approx 0.15 cm.

The downwave higher harmonic amplitude modulations are less pronounced in fig. 8 compared to fig. 3, when the tank was fully developed. Nonetheless, the BEM model does predict spatial amplitude modulations which are qualitatively similar to the experimental results. The degree of disagreement present is certainly also due to the influence of flow separation at the first harmonic frequency, as a misrepresentation of the first harmonic component will be passed on as erroneously simulated higher harmonics as well.

Conclusions

The spectral evolution of an incident regular wave train has been traced as it propagated over a submerged rectangular obstacle, and comparisons have been made between the experimental data and both a traditional linear scattering model and a BEM model. The experimental data revealed the existence of spatial amplitude modulations downwave of the obstacle.

The linear model of Losada (1991) was shown to predict the reflection coefficient quite well, despite the high degree of nonlinearity present in the vicinity of the obstacle. However, it was seen that the transmission coefficient was consistently overpredicted due the linear model's omission of energy transfer to higher harmonics and energy dissipation. An implication of the above results is that the linear scattering approach may underestimate the effectiveness of a structure (ie, submerged breakwater) under highly nonlinear situations.

The BEM model by Grilli *et al.* (1989) was found to simulate downwave spatial amplitude modulations qualitatively similar to those found in the data. Comparisons, however, were hampered by the presence of flow separation in the experiments which could not be modelled in the BEM formulation. It is conjectured that the BEM model would have simulated the experiments more ac-

curately, had the obstacle depth been greater, thus inducing less flow separation.

References

- Dold, J.W. and D.H. Peregrine (1984). Steep unsteady water waves: an efficient computational scheme. *Proceedings of the 19th International Coastal Engineering Conference*, ASCE, Houston, 955-967.
- Grilli, S.T., J. Skourup and I.A. Svendsen (1989). An efficient boundary element method for nonlinear water waves, *Engineering Analysis with Boundary Elements*, **6**, 97-107.
- Grilli, S.T. and I.A. Svendsen (1990) Corner Problems and Global Accuracy in the Boundary Element Solution of Nonlinear Wave Flows, *Engineering Analysis with Boundary Elements*, **7**(4), 178-195.
- Longuet-Higgins, M.S. and E.D. Cokelet (1976). The deformation of steep surface waves on water - I: a numerical method of computation, *Proceedings of the Royal Society of London*, **A350**, 1-26.
- Losada, I. (1991) Estudio de la propagacion de un tren lineal de ondas por un medio discontinuo, Ph.D. dissertation, University of Cantabria, Santander, Spain.
- Mei, C.C. and J.L. Black (1969). Scattering of surface waves by rectangular obstacles in waters of finite depth, *Journal of Fluid Mechanics*, **28**, 499-511.
- Rey, V., M. Belzons and E. Guazzelli (1991). Propagation of surface gravity waves over a rectangular submerged bar, *Journal of Fluid Mechanics*
- Seelig, W.N. (1980). Two-dimensional tests of wave transmission and reflection characteristics of laboratory breakwaters, Technical Report no. 80-1, USAE Coastal Engineering Research Center, Fort Belvoir, VA.
- Takano, K. (1960). Effets d'un obstacle parallelepipédique sur la propagation de la houle, *La Houille Blanche*, **2**, 247-267.

CHAPTER 87

THE SUBMERGED PLATE AS A WAVE FILTER

THE STABILITY OF THE PULSATING FLOW PHENOMENON

Dr.-Ing. Kai-Uwe Graw **

ABSTRACT

For many applications it is possible to reduce the wave motion in the protected area sufficiently using the submerged plate as a wave filter. The horizontal submerged plate, which hardly obstructs the cross-section of the flow, cannot be explained by the Wiegel approach at all. A strong pulsating flow opposite to the direction of the wave propagation originates beneath the plate during wave attack. New velocity measurements, carried out with an ultrasonic 3D-probe in the region below the plate, make it now possible to explain the principle much more in detail. They show that the flow phenomenon at the plate is very stable, the flow is nearly as strong if the region below the plate is partly closed.

1. REASONS FOR THE INVESTIGATIONS

The protection of coastlines and harbours against wave attack is mainly achieved by the use of solitary breakwaters. Their negative features are that they hinder:

- a) the water exchange between the open sea and the protected area (diverted sediment transport, deteriorated water quality) and
- b) the view over the open sea.

Underwater breakwaters are not visible, but the water exchange does not increase as much as the efficiency decreases. One possibility to enhance the performance without hindering the water exchange is the use of a semi-submerged vertical wall which obstructs the energy flux near the surface. However, this leads to construction problems (destruction of the

** Senior Research Engineer

Wasserbau und Wasserwirtschaft, Bergische Universität GH Wuppertal
Pauluskirchstraße 7, 5600 Wuppertal 2, Germany

wall in large waves), and also in this case the structure is visible. The breakwater type which reduces all these secondary problems is the rigid horizontal submerged plate mentioned in this paper. The plate cannot be used to stop the wave motion in the protected area, but its efficiency is sufficient for many applications.

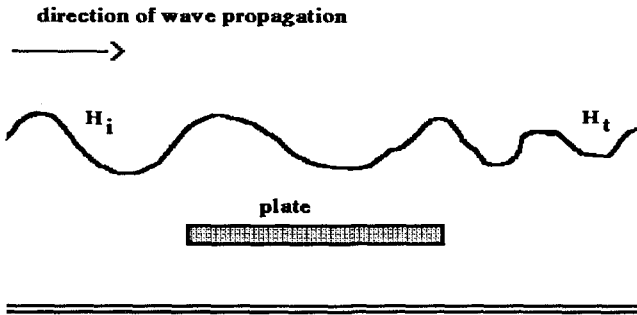


Figure 1: The submerged plate

2. THE SUBMERGED PLATE: THE WAVE FILTER

The performance of "normal" breakwaters can be explained by using the Wiegel approach. This means that the part of the wave energy in the regions covered by the structure is reflected, a very small part of the energy is dissipated at its surface and the other part passes by.

Figure 2 shows one series of the different measurements performed by Dauer [1984]. The figure shows the results for the shortest of the plates used (the length is only 1.333 times the water-depth, $l/d=1.333$).

The performance of the plate is not adequate in two cases:

- ① All long waves ($L/l > 6$) are not reduced sufficiently, the wave height reduction is approximately 25%.
- ② Furthermore it can be seen, that the plate which is submerged by more than one third (40%) of the water-depth does not really work.

All waves not longer than 3.5 times the plate length ($L/l < 3.5$) are reduced by more than 50%. The largest value of the wave height reduction is approximately 80%.

The best results were obtained for the three smallest values, but one important reason for this is wave breaking above the plate, connected with large forces exerted on the plate. For a submergence depth between 20 and 30% of the water depth a sufficient wave height reduction was observed, not caused by wave breaking. These results were confirmed for

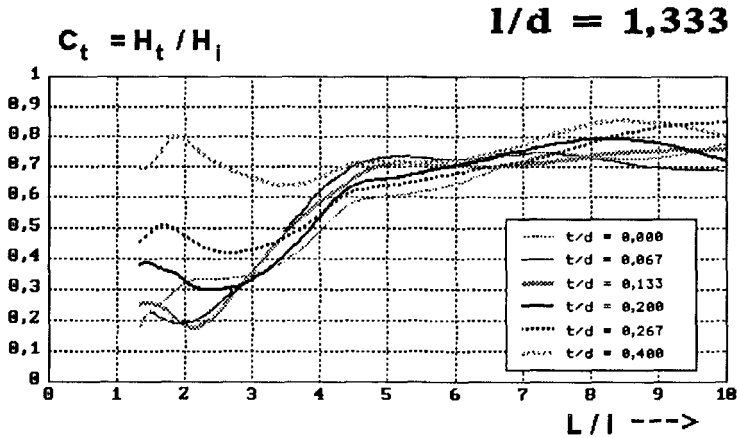


Figure 2: Wave height reduction at the plate [Dauer, 1984]

different plates longer than two times the wave length ($l/d > 2$). The wave height reduction is relatively constant (50 - 70%) in the wave length range between $L/l = 0.4$ and 4.

Examining a normal solitary breakwater, this principle is correct; looking at the semi-submerged vertical wall, it does not cover the whole problem but it is a good approximation. The horizontal submerged plate which hardly obstructs the cross-section of the flow cannot be explained by the Wiegel approach at all. For this reason, and as it performs well only in a particular region of the wave spectrum, it shall be called a wave filter from now on.

3. THE PULSATING FLOW

Dick [1968] noticed a flow around a horizontal plate submerged beneath waves, but he did not give any explanation for it. Analyses of the flow behaviour, based on flow visualization experiments [Graw, 1988; Graw, Kaldenhoff, Stieglmeier, 1989], and measurements of the wave height were presented by Hoeborn [1986]. She first gave an explanation based on a resonant flow behaviour. Continual experiments have shown that the dissipation of energy at the plate is caused in the wake behind the plate [Fischer, 1990; Fischer, Jirka, Kaldenhoff, 1991]. A finite element model gave us the possibility of calculating the energy equilibrium at the plate quite well, but the forecast of the flow was still uncertain. New velocity measurements, carried out with an ultrasonic 3D-probe in the region below the plate, make it now possible to explain the principle much more in detail. They show that the flow phenomenon at the plate is very stable, the flow is nearly as strong if the region below the plate is partly closed.